HHS Public Access

Author manuscript

Nat Neurosci. Author manuscript; available in PMC 2012 May 23.

Published in final edited form as:

Nat Neurosci. ; 14(10): 1317–1322. doi:10.1038/nn.2906.

Coordinated dynamic encoding in the retina using opposing forms of plasticity

David B. Kastner[1] and **Stephen A. Baccus**[2]

[1]Neuroscience Program Stanford University School of Medicine, 299 Campus Drive W., Stanford, CA, USA

[2]Department of Neurobiology, Stanford University School of Medicine, 299 Campus Drive W., Stanford, CA, USA

Abstract

The range of natural inputs encoded by a neuron often exceeds its dynamic range. To overcome this limitation, neural populations divide their inputs among different cell classes, as with rod and cone photoreceptors, and adapt by shifting their dynamic range. We report that the dynamic behavior of retinal ganglion cells in salamanders, mice, and rabbits is divided into two opposing forms of short-term plasticity in different cell classes. One population of cells exhibited sensitization—a persistent elevated sensitivity following a strong stimulus. This novel dynamic behavior compensates for the information loss caused by the known process of adaptation occurring in a separate cell population. The two populations divide the dynamic range of inputs, with sensitizing cells encoding weak signals, and adapting cells encoding strong signals. In the two populations, the linear, threshold and adaptive properties are linked to preserve responsiveness when stimulus statistics change, with one population maintaining the ability to respond when the other fails.

Adaptive systems adjust their response properties to the statistics of the recent input[1]. However, a fundamental tradeoff exists between optimizing for the current environment, and being able to respond reliably when the environment changes. Due to statistical limitations of how long it takes to estimate the recent stimulus distribution[2,3], the timescale of adaptation greatly exceeds the integration time of the response in many sensory systems[1,4–7]. As a consequence, when stimulus statistics change suddenly, as often occurs in natural scenes[8], sensory neurons often fall below threshold or saturate, until they successfully measure and adapt to the statistics of the new environment.

In the retina, a transition from a high to a low contrast environment reveals this tradeoff, when the decreased sensitivity caused by high contrast prevents the neuron from firing for some time after the contrast decreases[7,9,10]. Adapting primate retinal ganglion cells are known to recover their activity after high contrast with a prolonged time constant of ~ 6 s[11].

Author Contributions. D.B.K. and S.A.B. designed the study, D.B.K performed the experiments and analysis, and D.B.K and S.A.B. wrote the manuscript.

However, human psychophysical performance recovers faster at early timescales (< 1 s), matching an ideal observer model, indicating that some adapting neural pathway can signal quickly even after exposure to high contrast[12]. We recorded from retinal ganglion cells in amphibian and mammalian retina during sudden changes in the statistics of the stimulus to examine how neural populations maintain responsiveness when the environment changes.

RESULTS

Adaptation and Sensitization in retinal ganglion cells

We measured the average firing rate response of salamander, mouse, and rabbit ganglion cells to a contrast transition by presenting a spatially uniform visual stimulus. The intensity was drawn from a Gaussian white noise distribution with a constant mean and a standard deviation that alternated between high and low temporal contrasts (Fig. 1a). Even after a short high contrast presentation, many ganglion cells failed to respond for seconds after the transition to low contrast as their firing rate slowly recovered, consistent with previously reported properties of contrast adaptation[4,6,7,9,13] (Fig. 1a,b).

We found, however, that some neurons responded rapidly after a transition to low contrast (Fig. 1a), even after a long high contrast presentation (Fig. 1b). These cells exhibited an elevated response following high contrast that persisted for several seconds, gradually decreasing during low contrast. This decay had an average (± standard deviation) time constant of 2.4 ± 1.1 s in salamanders, 1.3 ± 0.3 s in mice, and 4.1 ± 2.7 s in rabbits.

To measure how the sensitivity of the two populations changed during low contrast, we computed a linear-nonlinear (LN) model of each neuron's firing rate[9] (see methods) (Supplementary Fig. 1). We compared the nonlinearities computed early (L_{early}) and late (L_{late}) after the transition to low contrast (bars in Fig. 1a). For the two populations of ganglion cells, the change in firing rate arose from a change in average sensitivity, defined as the average slope of the nonlinearity (Fig. 1c). For salamanders, cells that elevated their activity at the transition to low contrast doubled their average sensitivity (2.1 ± 0.3) during L_{early} relative to L_{late}. In part, a change in threshold underlaid this change in average sensitivity. Because the presence of a strong stimulus elevated the sensitivity to a subsequent weak stimulus, we term this property sensitization, by analogy to behavioral sensitization[14].

Sensitizing cells were found in salamanders (Fig. 1 a,c) (32%, 80 out of 250 cells), mice (Fig. 1 a,c) (12%, 5 out of 41 cells), and rabbits (21%, 8 out of 39 cells) (Supplementary Fig. 2a,b). A similar ratio of salamander ganglion cells has been reported in abstract form to respond to contrast decrements (C.A. Burlingame, A.Y. Dymarsky, M.J.Berry II, *Soc Neurosci. Abstr*. 506.11, 2007). Recording from many cell types in the salamander, we found that adapting and sensitizing cells formed two distinct classes (Fig. 1d). For each species, we used the nonlinearities during L_{early} and L_{late} to compute the average loss of sensitivity. The sensitivity loss in adapting cells during L_{early} correlated with the fraction of sensitizing cells in the species (Supplementary Fig. 2c), suggesting that sensitizing cells compensate for the sensitivity loss due to adaptation.

Sensitization occurred over a broad range of spatial frequencies and stimulus sizes (Supplementary Fig. 3). By measuring sensitivity after different high contrast durations, we found that after 0.55 s of high contrast, a cell reached 63 % of its peak sensitization (τ = 0.55 s) (Fig. 1e). Thus, significant sensitization is expected even during brief fixations. After the transition to low contrast, increased activity was not instantaneous, but reached a peak in 0.98 ± 0.03 s. This delay may reflect the statistical limitation necessitating sufficient temporal integration for any system to adapt to a contrast decrement[2,4,12].

We tested whether the two forms of plasticity generalized to statistics other than contrast by changing the mean luminance while keeping the contrast fixed. Each cell type showed consistent sensitizing or adapting behavior for changes in both stimulus parameters (Supplementary Fig. 4a,b, and Fig. 1f).

Adapting and sensitizing populations encode the same signals

Although adaptation and sensitization slowly modulated the average firing rate, retinal ganglion cells encode visual information on a much finer timescale using reproducible firing events—intervals of high firing probability lasting < 0.1 s in duration[9]. We compared firing events for adapting and sensitizing cells recorded simultaneously by repeating an identical stimulus sequence during L_{early} and L_{late}. During L_{late}, 94 % of adapting cell firing events occurred synchronously with a sensitizing cell firing event (Fig. 2a,b). Consistent with the changing nonlinearities, during these individual common firing events the activity of adapting cells during L_{early} decreased by 41 ± 3 % relative to L_{late} (n = 28), whereas the activity of sensitizing cells increased by 93 ± 8 % (n = 12). Thus, the two populations coordinated their encoding such that they responded to the same visual stimuli, with the representation shifting more to the sensitizing population during L_{early}.

To examine the specific messages encoded by sensitizing and adapting cells, we measured how the plasticity of a cell corresponded to its linear spatio-temporal receptive field (Fig. 2c,d). For all salamander Off-type cells—~90 % of the cells in the salamander retina[15]—the adaptive index divided each cell type into two groups, composed of both adapting and sensitizing cells. Within a cell class, the spatial receptive fields of adapting and sensitizing cells overlapped (Fig. 2e), but maintained a minimum spacing between members of the same class (Fig. 2f)[16]. This indicates that a mixed group of cells with highly similar linear receptive fields[15], splits into two classes with different short-term plasticity, each of which appears to tile the retina. Thus, adapting and sensitizing populations represent the same stimuli. In mice, sensitizing cells also comprised different cell types, including both On and Off classes (Supplementary Fig. 5a). In addition, some adapting and sensitizing cells in mice and rabbits had very similar temporal properties (Supplementary Fig. 5b).

Because sensitizing cells compensate for the loss of sensitivity in the adapting population during low contrast, we tested whether the reverse was true during high contrast. During H_{early}, 0.5 – 5 s after a transition to high contrast, the nonlinearity of sensitizing cells saturated (Supplementary Fig. 6), reaching 98 ± 1 % of their estimated maximal firing rate, and their sensitivity dropped to 10 ± 4% of the peak sensitivity (n = 3). Adapting cells did not saturate, however, and only reached 79 ± 4 % of their maximal rate while retaining 63 ±

8% of their peak sensitivity (n = 11). Thus, adapting cells compensated for saturation in the sensitizing population at the transition to high contrast.

Sensitizing cells preserve weak signals, adapting cells preserve strong signals

To measure the functional benefit of having the two opposing forms of plasticity, we quantified the discriminability (*d'*) in the combined population of sensitizing and adapting cells after a decrease in contrast (see methods). This measure derives from the Fisher information, an upper bound on the information available by any unbiased decoding scheme[17]. Discriminability, and Fisher information, increases with the slope of the nonlinearities at each input (Fig. 3a), but decreases with the variability of the response at that input. It also depends on correlations between cells, which can either increase or decrease information[18]. We used simultaneously recorded populations of adapting and sensitizing cells to account for the nonlinearities, variability, and covariance as a function of distance between cells (Supplementary Fig. 7) (see methods). Discriminability in the adapting population alone decreased 44.2 ± 1.9 % during L_{early} relative to L_{late}. However, for the combined population of sensitizing and adapting cells, discriminability only decreased 16.8 ± 2.3 % during L_{early}. Thus, the addition of sensitizing cells to the population substantially reduced the loss of discriminability when the contrast of the environment changed.

We then examined this improvement in discriminability in the full population at each separate stimulus, and found that the addition of sensitizing cells to a population of adapting cells enhanced the discriminability of weak signals (Fig. 3b). The improvement produced by including sensitizing cells during L_{early} was 1.8 times the improvement during L_{late}. Discriminability improved most in the region of reduced threshold of the nonlinearities of sensitizing cells, indicating that this reduction during L_{early} further enhanced the encoding of weak signals. Conversely, the addition of adapting cells to a population of sensitizing cells enhanced discriminability of strong signals (Fig. 3b). As expected, this contribution of adapting cells increased during L_{late} as their threshold decreased and sensitivity increased.

The dynamics of adapting and sensitizing cells decayed towards a steady-state response that depended on the contrast. To understand the endpoint of this adaptive process, we measured the steady-state nonlinear response curve from LN models computed across a ten-fold range of contrasts (Fig. 4a). Compared to adapting cells, sensitizing cells had a threshold closer to the mean (Fig. 4a,b). Thus, across all contrasts the two populations divided the range of inputs, with sensitizing cells encoding weak signals, and adapting cells encoding strong signals.

Consistent with this division of labor, sensitizing cells had a larger center and weaker surround than did adapting cells (Fig. 2c). This difference likely enables sensitizing cells to improve their signal to noise ratio for weak inputs by spatial averaging, as occurs for ganglion cells during low luminance conditions[19,20].

Ideal normalization and contrast estimation

To explain the relationship between contrast and the steady-state dynamic range of adapting and sensitizing cells, we considered that an ideal encoder that maximizes information from a stimulus distribution should change its sensitivity inversely with the contrast[1]. This ideal normalization is thought not to occur in the retina because ganglion cells reduce their sensitivity by a fraction less than the change in contrast. This can be seen by comparing nonlinearities whose input has been normalized by the contrast (Fig. 4b top)[7,21]. We found, however, that a model, M_α (see methods), using ideal normalization does account for steady-state adaptation, causing the normalized curves to nearly overlay, if one considers that the rescaling occurs after a threshold (Fig. 4b bottom). This type of normalization could occur if the stimulus passes through a threshold, such as from voltage-dependent Ca channels in bipolar cell presynaptic terminals[22], and then rescaling occurs about that threshold (Fig. 4c).

Estimation of contrast in an uncertain environment

A change in stimulus statistics, as has recently occurred during L_{early}, necessarily brings uncertainty as to the new range of inputs[2–4]. As seen in the different dynamics of their firing rates (Fig. 1a) and nonlinearities (Fig. 1c), the two populations make different choices during that time of uncertainty, and then adjust their response to the new contrast. Thus, we can view the initial placement of the nonlinearity as corresponding to an initial estimate of the contrast. The model M_α represents an idealized relationship between contrast and the optimized response of a cell to that contrast. We therefore used the model as a lookup table to identify the contrast estimate given the nonlinearity of a cell at different times during low contrast (Fig. 4d). We mapped nonlinearities for each cell at different time intervals to a given estimated contrast by finding the most similar nonlinearity in the steady-state model M_α. During L_{early}, adapting cells overestimated the contrast at 1.6 ± 0.1 times the actual value (n = 12), and sensitizing cells underestimated the contrast at 0.5 ± 0.1 times the actual value (n = 6).

Variability and threshold correspond in the two populations

We next sought to explain why sensitizing cells raised their threshold during prolonged exposure to the low contrast environment, rather than maintaining a continued higher firing rate during low contrast. For optimal encoding of an input, the level of noise can influence the placement of threshold, with higher noise necessitating a higher threshold[23]. Sensitizing cells had lower variability than adapting cells as measured by the Fano factor, or variance to mean ratio, by a factor of 1.86 ± 0.17 (Supplementary Fig. 8a). This may occur in part due to their different receptive field sizes, which would predict, assuming independent noise from photoreceptors, that their variability would differ by the ratio of the receptive field areas, which was 2.07 ± 0.06 (26 sensitizing and 74 adapting cells).

We then examined the parameters of the model M_α, which resembles an ideal observer model of human perception having ideal contrast normalization with a threshold set by internal noise[12]. Compared to adapting cells, sensitizing cells had a lower initial threshold, α (by a factor of 1.96) and a lower final threshold, θ, (by a factor of 3.6) (Supplementary Fig. 8b), possibly constrained by the different variability in the two populations. Because of this connection between variability and threshold, and the defined relationship of the steady-state

threshold with contrast (Fig. 4a–c), we considered that after a change in contrast, the threshold might then become optimized in the steady state to convey greater information about the current stimulus.

Sensitizing cells decrease activity but convey more information

These observations led us to propose that during low contrast, from L_{early} to L_{late}, information transmission improved for both adapting and sensitizing cells, even though the firing rates of the two populations moved in opposite directions. We thus measured the mutual information during L_{early} and L_{late} for adapting and sensitizing cells by presenting pulses of eight different intensities during L_{early} and L_{late} (Fig. 5a). As expected, adapting cells conveyed less information during L_{early} than sensitizing cells, and increased their information transmission between L_{early} and L_{late}. Remarkably, we found that sensitizing cells also conveyed more information during L_{late} than L_{early} (Fig. 5b) even though their activity decreased during L_{late} (Supplementary Fig. 9a). Thus, the increase in threshold for sensitizing cells from L_{early} and L_{late} improves information transmission. This increase in mutual information was consistent with the population measurement of discriminability (Fig. 3b), in that the sensitizing population alone lost 8.4 ± 4.0 % of its discriminability during L_{early}. Thus although both sensitizing and adapting cells lose information at the transition to low contrast, sensitizing cells lose much less.

This loss of information in the sensitizing population despite the increase in firing rate can be explained by comparing the variability during L_{early} and L_{late}. A lower threshold during L_{early} exposed an increase in noise at the weakest stimuli for sensitizing cells (Fig. 5c), but not for adapting cells (Supplementary Fig. 9c), confirming that subthreshold noise limits the steady-state placement of threshold. Previously, it has been shown that higher firing rate correlates with greater information transmission[24,25]. Here, however, the decay in activity in sensitizing cells actually improves the encoding of the low contrast stimulus.

To further examine how encoding changed for individual stimuli, we computed the stimulus-specific information[26] (see methods), during L_{early} and L_{late}. This measure reflects the contribution of each specific stimulus to the mutual information. During both L_{early} and L_{late}, adapting and sensitizing cells favored different ends of the input signals (Fig. 5d), with sensitizing cells conveying the greatest amount of information about the weakest stimuli during L_{early}. This was consistent with the measure of discriminability, which showed that the additional discriminability conveyed by the two populations separated during L_{early} (Fig. 3b). However, across all stimuli, information transmission improved from L_{early} to L_{late}. Thus, after the initial opposing thresholds chosen by sensitizing and adapting cells, both populations improved their information transmission with more prolonged exposure to a steady environment.

Discussion

These results give an explanation for the opposing dynamics of sensitizing and adapting cells. A decrease in contrast creates the greatest ambiguity as to the statistics of the stimulus, because the new range of inputs only contains weak signals that fall within the most probable values of the previous distribution[2,4]. The addition of sensitizing cells to the

population improves the encoding of weak signals, with the greatest improvement being after the contrast decrease (Fig. 3b). However, neither population perfectly encodes the new distribution after the contrast decreases (Fig. 5 b,d), a condition compelled by the uncertainty that accompanies a transition to an environment of weak signals[2,4]. But by positioning their sensitivity at different sides of the steady-state value, sensitizing and adapting cells bracket the target sensitivity by underestimating or overestimating, respectively, the steady-state sensitivity (Fig. 4d). Thus, during the time of greatest statistical uncertainty the two populations span the range of inputs. Because this initial position deviates from optimal, both sensitizing and adapting cells then increase their information transmission by adopting their steady-state positions (Fig. 5b,d). Therefore, the coordinated dynamics of adapting and sensitizing cells (Fig. 1a) represent a tradeoff between the immediate encoding of an uncertain distribution and the delayed optimization for that distribution.

Dynamic changes within the circuitry of the inner retina underlie contrast adaptation[9,27–29]. Two adapting pathways, one excitatory and one inhibitory could combine to produce sensitization (Fig. 6). In this scheme, high contrast causes inhibitory transmission to adapt. Then, at the transition to low contrast, the residual lowered inhibition raises sensitivity (Fig. 6b,c). This model of sensitization indicates that sensitizing cells receive a negative version of an adapting cell's response. This causes the two populations to encode different signals, in particular during the time when each population has the highest likelihood of failing to encode the stimulus. The model also indicates that the source of increased variability during sensitization lies prior to the initial threshold in the excitatory pathway, as decreased inhibition prior to this threshold could result in greater transmission of noise.

A neuron with a response curve that spans its distribution of inputs will encode those inputs efficiently[1]. However, to perform this task dynamically would require that the neuron maintain its threshold to encode the weakest signals, and its maximal response to encode the strongest, making both ends of the response curve vulnerable to saturation should the stimulus distribution change. Here, we have shown that the retina divides this problem in two, with linear filtering, threshold placement, and dynamic plasticity combining to encode a specific range of inputs. Low threshold cells with weaker surrounds sensitize to reliably encode weak signals. High threshold cells with stronger surrounds adapt to reliably encode strong signals. When one population saturates, the other compensates. The ability to coordinate opposing forms of dynamic encoding allows a neural population to avoid the inherent losses of any single type of plasticity.

Methods

Experimental preparation

We recorded from retinal ganglion cells of larval tiger salamanders, mice and rabbits using an array of 60 electrodes (Multichannel Systems) as described[9]. Ringer solution (124 mM NaCl, 2.6 mM KCl, 2 mM $CaCl_2$, 2 mM $MgCl_2$, 1.25 mM NaH_2PO_4, 26 mM $NaHCO_3$, 22.2 mM glucose) perfused the mouse retina at 32 – 35 °C and the solution maintained a pH of 7.35 – 7.4 by aeration with 95/5 % O_2/CO_2. Ames' medium perfused the rabbit retina at 37 °C.

A video monitor projected the visual stimuli at 30 Hz using Psychophysics Toolbox in Matlab. Stimuli were uniform field with a constant mean intensity, *M*, of 8 – 10 mW/m^2 and were drawn from a Gaussian distribution unless otherwise noted. Contrast is defined as σ =*W*/*M*, where *W* is the standard deviation of the intensity distribution, unless otherwise noted. To measure changes in firing rate for adapting and sensitizing cells (Fig 1a), for salamander, 80 trials were presented, alternating between 4 s high (35 %) and 16 s low contrast (5 %). For mouse, 104 trials were presented of 15 s high (30 %) and 15 s low contrast (9 %). For the measurement of the average time to the first spike after the transition to low contrast (Fig. 1b), results were pooled over 5 experiments, with > 50 trials for each cell. To measure the development of sensitization (Fig. 1e), conditions were interleaved in blocks of 17 trials for a total of 102 trials in each condition.

Linear-Nonlinear models

LN models (Supplementary Fig. 1) consisted of the light intensity passed through a linear temporal filter, which describes the average response to a brief flash of light, followed by a static nonlinearity, which describes the threshold and sensitivity of the cell. To compute the model, the stimulus, *s*(*t*), was convolved with a linear temporal filter, *F* (*t*), which was computed as the time reverse of the spike triggered average stimulus, such that

$$g(t) = \int F(t-\tau)\, s(\tau)\, d\tau. \quad (1)$$

A static nonlinearity, *N* (*g*), was computed by comparing all values of the firing rate, *r* (*t*) with *g*(*t*)and then computing the average value of *r* (*t*)over bins of *g*(*t*). The filter, *F* (*t*), was normalized in amplitude such that it did not amplify the stimulus, i.e. the variance of *s* and *g* were equal[9]. Thus, the linear filter contained only relative temporal sensitivity, and the nonlinearity represented the overall sensitivity of the transformation. Adapting and sensitizing cells were equally well fit by an LN model. Model and data had a correlation coefficient of 56 ± 2 % for adapting cells, and 61 ± 3 % for sensitizing cells.

The sigmoidal function used to fit the nonlinearities was

$$y = x_0 + \frac{m}{1+\exp\left(\frac{x_{1/2}-x}{r}\right)}, \quad (2)$$

where x_0 is the basal firing rate, *m* is the maximal firing rate, $x_{1/2}$ is the x value at 50 % of maximal firing, and *r* controls the maximal slope.

Adaptive index

The adaptive index was $A = \frac{r_{early} - r_{late}}{r_{early} + r_{late}}$, where r_{early} and r_{late} are the firing rates during a 3 s window beginning during L_{early} and L_{late}, respectively. Only cells that responded during r_{early} and r_{late} were included.

Receptive fields

Spatio-temporal receptive fields were measured in one or two dimensions by the standard method of reverse correlation[30] of the spiking response with a visual stimulus consisting of either lines or squares. The spatio-temporal receptive field was approximated as the product of a spatial profile and a temporal filter[31]. The normalized distance between receptive fields (Fig. 2f) was the spacing, $S = d/(r_1 + r_2)$, where d is the distance between the center of the two cells, and r_1 and r_2 are the radii of the two cells along the line connecting their centers.

Discriminability

The average discriminability between nearby stimuli[17] as a function of the stimulus was estimated as:

$$d'(g) = \sqrt{(I_F(g)}, \quad (3)$$

where I_F, the Fisher information, was computed as,

$$I_F(g) = \mathbf{N}'(g)^{\mathrm{T}}\mathbf{Q}(g)^{-1}\mathbf{N}'(g) + \frac{1}{2}\mathrm{Tr}\left[\mathbf{Q}'(g)\,\mathbf{Q}^{-1}(g)\,\mathbf{Q}'(g)\,\mathbf{Q}^{-1}(g)\right]. \quad (4)$$

Total discriminability was computed as $d' = \int d'(g)dg$. The vector $\mathrm{N}'(g)$ is the derivative of the nonlinearity for a population of cells with respect to the filtered stimulus g, $\mathbf{Q}g$ is the covariance matrix as a function g, and the function Tr is the trace of a matrix[18]. Nonlinearities, $\mathbf{N}g$, were sigmoidal fits to the measured nonlinearities. The diagonal terms of $\mathbf{Q}g$, which were the variance of each cell as a function of the stimulus g, were empirically well fit by a combination of multiplicative noise β that depended on g, and additive noise γ that was independent of g. This relationship was fit to the data (Fig. 5c and Supplementary Fig. 9c) for sensitizing and adapting cells during L_{early} and L_{late},

$$Q_{ii}(g) = \beta N_i(g) + \gamma. \quad (5)$$

Only sensitizing cells had significant additive noise. The off-diagonal terms of $\mathbf{Q}(g)$, the covariance between cells, were well fit by the geometric mean of the two variances weighted by distance (Supplementary Fig. 7a),

$$Q_{ij}(g) = c(d_{ij})\ \sqrt{Q_{ii}(g)\,Q_{jj}(g)}. \quad (6)$$

The correlation coefficient $c(d_{ij})$ decayed exponentially as a function of distance between two cells (Supplementary Fig. 7b). Different functions $c(d_{ij})$ fit during L_{early} and L_{late} for pairing within and between adapting and sensitizing cells. The fractional loss in discriminability during L_{early} was $1 - \left(d'_{early}/d'_{late}\right)$. Distance values d_{ij} were taken from a complete population of sensitizing and adapting cells spanning ~1 mm (Fig. 2e). Error was computed by multiple random draws from a set of 21 adapting and 13 sensitizing cells.

Models of contrast normalization

Nonlinearities, $N_\sigma(g)$, were computed across 12 steady-state contrasts ranging from 3 – 36 %. The basic model of normalization by the contrast, M_σ, was computed as:

$$M_\sigma = \hat{N}\left(\frac{g}{\sigma}\right), \quad (7)$$

where σ is the contrast, and a single function $\hat{N}(\ )$ was chosen to minimize the error between model and data, E_σ, defined as the average rms difference between the model and the set of nonlinearities, N_σ. The model of normalization following a threshold, M_α, was computed as:

$$M_\alpha = \hat{N}\left(\frac{U_\alpha(g)}{\sigma}\right), \quad (8)$$

where U_α is a threshold function. In practice, because the threshold of U_α was nearly always lower than that of $\hat{N}$, U_α could be substituted with a simpler form having a single parameter, α,

$$M_\alpha = \hat{N}\left(\frac{g-\alpha}{\sigma}\right). \quad (9)$$

The nonlinearity $\hat{N}(\ )$ and α were similarly chosen to minimize the error, E_α. The model normalizing each curve separately, M_{full}, was computed as:

$$M_{full} = \hat{N}\left(\frac{g-\alpha(\sigma)}{c(\sigma)}\right), \quad (10)$$

where in addition to a single $\hat{N}(\ )$, a separate α and c were chosen for each N_σ to minimize the error, E_{full}. For all models sigmoid fits to the data were used for N_σ. We compared the relative performance of M_α to M_σ and M_{full} by computing $(E_\sigma - E_\alpha)/E_\sigma - E_{full}$. Relative to M_σ, the single parameter model M_α captured 92.6 ± 1.0 % for adapting cells (n=40) and 85.6 ± 1.8 % for sensitizing cells (n = 12), of the error reduction produced by M_{full}, which contained 22 parameters.

Thresholds were computed from a fit to a nonlinearity using the equation:

$$N(x) = \begin{cases} 0 & x < \theta \\ ax - \theta & x \geq \theta \end{cases}, \quad (11)$$

where θ is the threshold, and a is the slope above threshold. The line above threshold was fit below saturating levels of the nonlinearity.

Information theory

To gather sufficient data to compute the mutual information after a transition to low contrast, L_{early} intervals occurred in different periods than L_{late}. To gather data for L_{early}, the stimulus alternated between 20 s of identical high contrast pulses and 2 s of low contrast containing 8 randomly chosen stimulus intensities. To gather data for L_{late}, the stimulus

consisted of a continuous 44 s sequence of random low contrast pulses. L_{early} and L_{late} conditions were alternated every 180 s. The response to stimulus pulses separated by 0.5 s was defined as a series of spike counts in bins of duration 150 ms (Fig. 5a), or in durations ranging from 10 – 150 ms (Supplementary Fig. 9b). Each response spanned a window of 150 ms, which included all spikes from a given pulse of the stimulus. Mutual information was computed by taking the difference between the total response entropy, $H(R)$, and the noise entropy, $H(R|S)$, where the entropy (H) is

$$H(X) = -\sum_x p(x) \log_2 p(x). \quad (12)$$

The stimulus specific information (I_{SSI}) was computed as:

$$I_{ISS}(s) = \sum_r p(r|s) \{H(S) = H(S|r)\}. \quad (13)$$

This measure is the average reduction of uncertainty gained from a measurement of the set of responses given a particular stimulus s[26]. The weighted average I_{SSI} over all stimuli is the mutual information between stimulus and response. All information measurements were corrected for limited data by computing the information for fractions of the data and then extrapolating the result to infinite data[32,33] (see Supplementary Fig. 9d).

Sensitization model

The model for sensitization was generated to reproduce the qualitative behavior of sensitizing cells. Excitatory and inhibitory adapting pathways were linked by a synaptic pathway. A prime candidate for the proposed inhibitory pathway could be the signal passed through amacrine cells, inhibitory interneurons in the retina[34]. Variables correspond to symbols in Fig. 6. The biphasic linear filter for both pathways matched the time to peak of sensitizing cells,

$$g(t) = \int L(t-\tau)\, s(\tau)\, d\tau \quad (14)$$

For the inhibitory pathway, a linear-threshold function contained a threshold set at the mean of the input $g(t)$,

$$u(t) = N_I(g) = \begin{cases} 0 & g < \langle g \rangle \\ g(t) - \langle g \rangle & g \geq \langle g \rangle \end{cases} \quad (15)$$

Brackets $\langle \ldots \rangle$ denote the average quantity. Adaptation occurred through a feedforward divisive operation. This adaptation could either occur at the level of a bipolar or amacrine cells[9]. The input $u(t)$was convolved with an exponential filter, F_A, and then $u(t)$ was divided by the result. A constant term in the denominator set the magnitude of adaptation,

$$v(t) = A_I(u(t)) = \frac{u(t)}{2 + \int F_A(t-\tau)\, u(\tau)\, d\tau}. \quad (16)$$

The time constant of F_A, representing the timescale of integration of the contrast, was 2 s,

$$F_A(t) = 0.5e^{\frac{-t}{2s}}. \quad (17)$$

The connection between the two pathways contained a temporal filter L_Q defined as an alpha function with a time to peak of 150 ms,

$$\begin{aligned} L_Q(x) &= \frac{2x}{.15}\exp\left(\frac{-(x-.15)}{.15}\right) \\ w_L(t) &= \int L_Q(t-\tau)\, v(\tau)\, d\tau. \end{aligned} \quad (18)$$

This delay could result from the action of metabotropic GABA receptors[35]. The connection between the two pathways also contained a saturating nonlinearity N_Q,

$$w(t) = N_Q(w_L(t)) = \frac{0.3}{1+\exp\left(\frac{0.03-w_L(t)}{0.01}\right)}, \quad (19)$$

the effect of which was to diminish the modulation of inhibitory transmission at high contrast, and amplify the modulation at low contrast. This saturation could arise from either synaptic depression or receptor desensitization[36]. An alternative source of the inhibitory pathway could be that adaptation is in the bipolar cell, and the delay and saturation (L_Q and N_Q) are produced by the filtering and membrane properties of an intervening amacrine cell[9].

The two pathways combined linearly,

$$x(t) = g(t) - w(t). \quad (20)$$

The pathways combined prior to the excitatory pathway threshold indicating that the amacrine cell might synapse presynaptically onto a bipolar cell terminal. The nonlinearity N_E in the excitatory pathway was a linear-threshold function with threshold α, representing the initial threshold α in the model M_α in Fig. 3,

$$y(t) = N_E(x(t)) = \left\{ \begin{array}{c|l} 0 & x(t) < \langle x(t)\rangle + \alpha \\ x(t) - (\langle x(t)\rangle + \alpha) & x(t) \geq \langle x(t)\rangle + \alpha \end{array} \right., \quad (21)$$

with α set to 0.025. Finally, the excitatory input $y(t)$ was passed through another stage of divisive adaptation, and the result thresholded by an output nonlinearity N_F. The threshold θ represented the final threshold θ of the model M_α from Fig. 3,

$$\begin{aligned} z(t) = \; & N_F(A_E(y(t))) = N_F\left(\frac{y(t)}{3+\int F_A(t-\tau)\, y(\tau)\, d\tau}\right) \\ & N_F(x) = \left\{ \begin{array}{c|l} 0 & x < \theta \\ x & x \geq \theta \end{array} \right. . \end{aligned} \quad (22)$$

θ was set to 0.005.

Error indicates standard error of the mean, computed across cells, unless otherwise noted.

Supplementary Material

Refer to Web version on PubMed Central for supplementary material.

Acknowledgments

We thank E. Knudsen and W.T. Newsome for comments on the manuscript, D. Baylor, R. W. Tsien, B. Wandell, P. Jadzinsky, A.L. Fairhall, F. Rieke, D. S. Fisher, and K.D. Miller for helpful discussions, and Y. Ozuysal and A. Huberman for technical assistance. This work was supported by grants from the NEI, Pew Charitable Trusts, McKnight Endowment Fund for Neuroscience, the Karl Kirchgessner Foundation, and the Alfred P. Sloan Foundation (S.A.B.); by the Stanford Medical Scientist Training Program, and an NSF IGERT graduate fellowship (D.B.K). Rabbit experiments were performed in the laboratory of Markus Meister at Harvard University.

References

1. Laughlin S. A simple coding procedure enhances a neuron's information capacity. Z Naturforsch, C, Biosci. 1981; 36:910–912.
2. DeWeese M, Zador A. Asymmetric dynamics in optimal variance adaptation. Neural Computation. 1998; 10:1179–1202.
3. Wark B, Fairhall A, Rieke F. Timescales of inference in visual adaptation. Neuron. 2009; 61:750–761. [PubMed: 19285471]
4. Fairhall AL, Lewen GD, Bialek W, de Ruyter van Steveninck RR. Efficiency and ambiguity in an adaptive neural code. Nature. 2001; 412:787–792. [PubMed: 11518957]
5. Nagel KI, Doupe AJ. Temporal processing and adaptation in the songbird auditory forebrain. Neuron. 2006; 51:845–859. [PubMed: 16982428]
6. Maravall M, Petersen RS, Fairhall AL, Arabzadeh E, Diamond ME. Shifts in coding properties and maintenance of information transmission during adaptation in barrel cortex. PLoS Biol. 2007; 5:e19. [PubMed: 17253902]
7. Smirnakis SM, Berry MJ, Warland DK, Bialek W, Meister M. Adaptation of retinal processing to image contrast and spatial scale. Nature. 1997; 386:69–73. [PubMed: 9052781]
8. Frazor RA, Geisler WS. Local luminance and contrast in natural images. Vision Res. 2006; 46:1585–1598. [PubMed: 16403546]
9. Baccus SA, Meister M. Fast and Slow Contrast Adaptation in Retinal Circuitry. Neuron. 2002; 36:909–919. [PubMed: 12467594]
10. Rieke F, Rudd ME. The Challenges Natural Images Pose for Visual Adaptation. Neuron. 2009; 64:605–616. [PubMed: 20005818]
11. Solomon SG, Peirce JW, Dhruv NT, Lennie P. Profound contrast adaptation early in the visual pathway. Neuron. 2004; 42:155–162. [PubMed: 15066272]
12. Snippe HP, van Hateren JH. Recovery from contrast adaptation matches ideal-observer predictions. J Opt Soc Am A Opt Image Sci Vis. 2003; 20:1321–1330. [PubMed: 12868637]
13. Brown SP, Masland RH. Spatial scale and cellular substrate of contrast adaptation by retinal ganglion cells. Nat Neurosci. 2001; 4:44–51. [PubMed: 11135644]
14. Pinsker HM, Hening WA, Carew TJ, Kandel ER. Long-term sensitization of a defensive withdrawal reflex in Aplysia. Science. 1973; 182:1039–1042. [PubMed: 4748675]
15. Segev R, Puchalla J, Berry MJ. Functional organization of ganglion cells in the salamander retina. J Neurophysiol. 2006; 95:2277–2292. [PubMed: 16306176]
16. Huberman AD, et al. Architecture and activity-mediated refinement of axonal projections from a mosaic of genetically identified retinal ganglion cells. Neuron. 2008; 59:425–438. [PubMed: 18701068]
17. Dayan, P.; Abbott, LF. Theoretical neuroscience: computational and mathematical modeling of neural systems. Vol. 460. MIT Press; 2009.
18. Abbott LF, Dayan P. The effect of correlated variability on the accuracy of a population code. Neural Computation. 1999; 11:91–101. [PubMed: 9950724]

19. Enroth-Cugell C, Robson JG. The contrast sensitivity of retinal ganglion cells of the cat. The Journal of Physiology. 1966; 187:517–552. [PubMed: 16783910]
20. Srinivasan MV, Laughlin SB, Dubs AT. Predictive Coding: A Fresh View of Inhibition in the Retina. Proceedings of the Royal Society of London. Series B, Biological Sciences. 1982; 216:427–459.
21. Chander D, Chichilnisky EJ. Adaptation to temporal contrast in primate and salamander retina. J Neurosci. 2001; 21:9904–9916. [PubMed: 11739598]
22. Mennerick S, Matthews G. Ultrafast exocytosis elicited by calcium current in synaptic terminals of retinal bipolar neurons. Neuron. 1996; 17:1241–1249. [PubMed: 8982170]
23. Field GD, Rieke F. Nonlinear signal transfer from mouse rods to bipolar cells and implications for visual sensitivity. Neuron. 2002; 34:773–785. [PubMed: 12062023]
24. Reinagel P, Reid RC. Temporal coding of visual information in the thalamus. J Neurosci. 2000; 20:5392–5400. [PubMed: 10884324]
25. Wessel R, Koch C, Gabbiani F. Coding of time-varying electric field amplitude modulations in a wave-type electric fish. J Neurophysiol. 1996; 75:2280–2293. [PubMed: 8793741]
26. Butts DA. How much information is associated with a particular stimulus? Network. 2003; 14:177–187. [PubMed: 12790180]
27. Kim KJ, Rieke F. Slow Na+ inactivation and variance adaptation in salamander retinal ganglion cells. J Neurosci. 2003; 23:1506–1516. [PubMed: 12598639]
28. Manookin MB, Demb JB. Presynaptic mechanism for slow contrast adaptation in mammalian retinal ganglion cells. Neuron. 2006; 50:453–464. [PubMed: 16675399]
29. Rieke F. Temporal contrast adaptation in salamander bipolar cells. J Neurosci. 2001; 21:9445–9454. [PubMed: 11717378]
30. Chichilnisky EJ. A simple white noise analysis of neuronal light responses. Network. 2001; 12:199–213. [PubMed: 11405422]
31. Olveczky BP, Baccus SA, Meister M. Segregation of object and background motion in the retina. Nature. 2003; 423:401–408. [PubMed: 12754524]
32. Gollisch T, Meister M. Rapid neural coding in the retina with relative spike latencies. Science. 2008; 319:1108–1111. [PubMed: 18292344]
33. Strong S, Koberle R, de Ruyter van Steveninck R. Entropy and Information in Neural Spike Trains. Phys Rev Lett. 1998
34. Baccus SA. Timing and computation in inner retinal circuitry. Annu Rev Physiol. 2007; 69:271–290. [PubMed: 17059359]
35. Maguire G, Maple B, Lukasiewicz P, Werblin F. Gamma-aminobutyrate type B receptor modulation of L-type calcium channel current at bipolar cell terminals in the retina of the tiger salamander. Proc Natl Acad Sci USA. 1989; 86:10144–10147. [PubMed: 2557620]
36. Li G-L, Vigh J, Gersdorff, von H. Short-term depression at the reciprocal synapses between a retinal bipolar cell terminal and amacrine cells. J Neurosci. 2007; 27:7377–7385. [PubMed: 17626198]

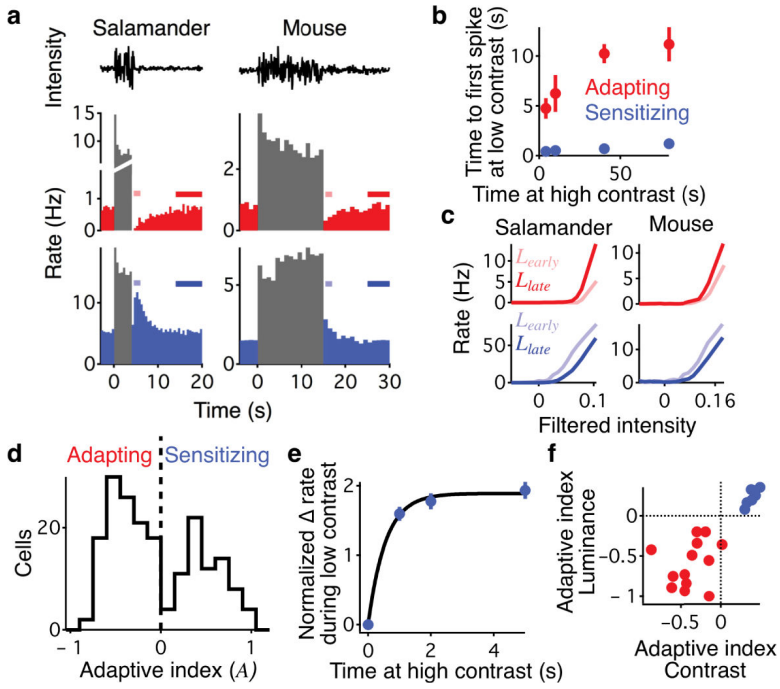

Figure 1.

Adaptation and sensitization in separate neural populations. (**a**) Stimulus intensity alternating between high and low contrast during a single trial (top), for salamander (left) and mouse (right). Firing rate response for adapting (middle) and sensitizing (bottom) cells, averaged over all trials, each with a different stimulus sequence. Color indicates response to low contrast. (**b**) Average time to first spike after a transition from high to low contrast (n = 2 – 12 cells). (**c**) Nonlinearities of an LN model (see methods) for cells in (**a**) calculated during intervals indicated by bars in (**a**) for salamander (left) and mouse (right). The interval L_{early} was defined as 0.5 – 2 s after the transition to low contrast, and L_{late} was 10 – 16 s for salamander and 10 – 15 s for mouse. (**d**) Adaptive indices (see methods) for 190 ganglion cells from 16 salamander retinas. The distribution is significantly bimodal (Hartigan's dip test, $P < 0.05$). (**e**) High contrast (35 %) was presented for 1, 2 or 5 s, followed by low contrast (3 %) for 15 s. The average change in firing rate between L_{early} and L_{late} is shown normalized by the average rate for low contrast in all conditions (n = 5 cells). Black line is an exponential fit to the data. (**f**) For the same cells, the adaptive index was computed separately for changing contrast at a fixed luminance, and compared to the adaptive index when changing the mean luminance a factor of 16 at a fixed contrast of 10 % (see Supplementary Fig. 4).

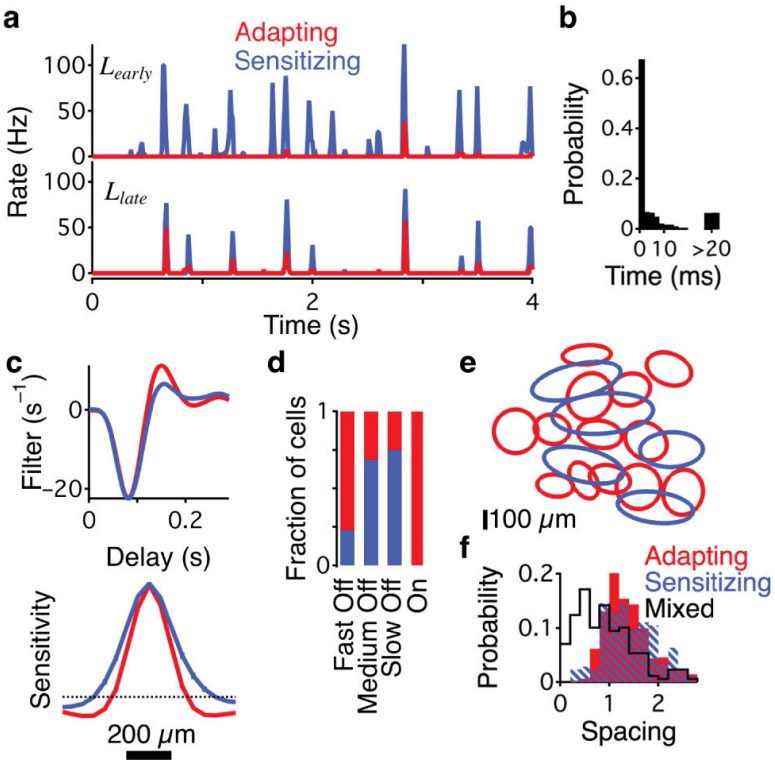

Figure 2.

Sensitizing and adapting populations encode common stimulus features. (**a**) Average response of salamander adapting and sensitizing cells to 26 trials of the same stimulus repeated during *Learly* and L_{late} after 4 s of high contrast (35%). Low contrast was 3–5 %. Firing rate binned at 10 ms. (**b**) Absolute difference in time between events in all pairs of fast Off-type adapting cells (n = 28) and sensitizing cells (n = 12). Events defined as times when a cell's firing rate, binned at 10 ms, exceeded 20 Hz. (**c**) Average temporal (top) and spatial (bottom) filters for adapting (n = 142), and sensitizing (n = 48) fast Off cells, mapped in one dimension. Curves obscure the error bars located at the peak and trough of the temporal filters and along the spatial filters. Spatial filters normalized to their peaks. (**d**) Fractions of adapting and sensitizing cells of different cell types, as classified by a cell's temporal filter (n = 209 fast Off, 16 medium Off, 20 slow Off, 9 On) (Supplementary Fig. 10). (**e**) Spatial receptive field centers of fast Off adapting and sensitizing cells recorded simultaneously. Receptive fields displayed at one standard deviation of a 2-D Gaussian fit. (**f**) Histogram of spacing (see methods) between nearest neighbors of fast Off adapting (n = 615) and sensitizing cells (n = 171).

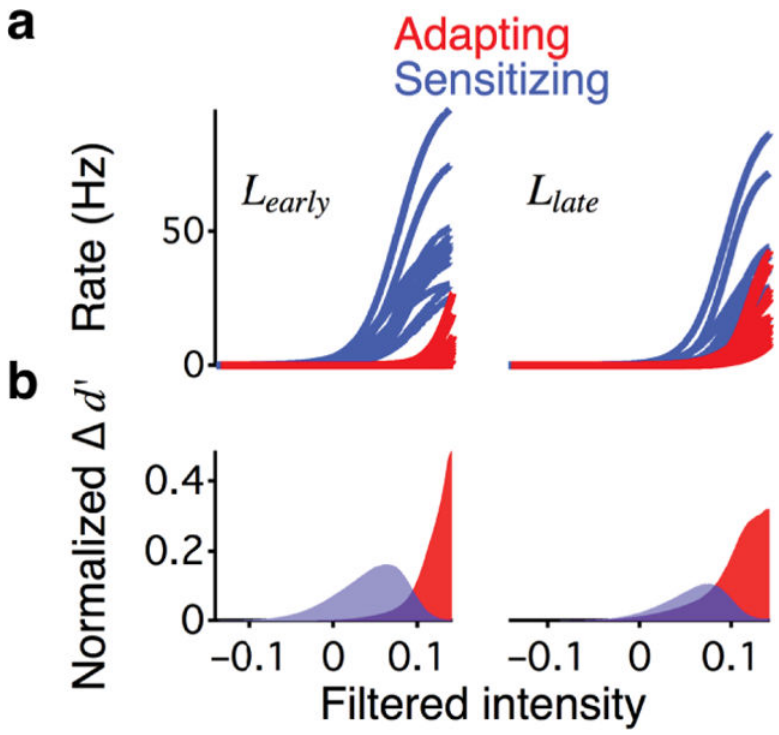

Figure 3.

Improvement of discriminability in a combined population of sensitizing and adapting cells. (**a**) Nonlinearities for adapting (n = 21) and sensitizing (n = 13) cells during *Learly* (left) and L_{late} (right). (**b**) Discriminability between nearby stimuli $d'(g)$ as a function of the stimulus (see methods) in the full population minus $d'(g)$ for the adapting population alone (blue) or minus $d'(g)$ for the sensitizing population alone (red) during L_{early} (left) and L_{late} (right). All values were normalized by the area of the total d' in the full population during L_{late}.

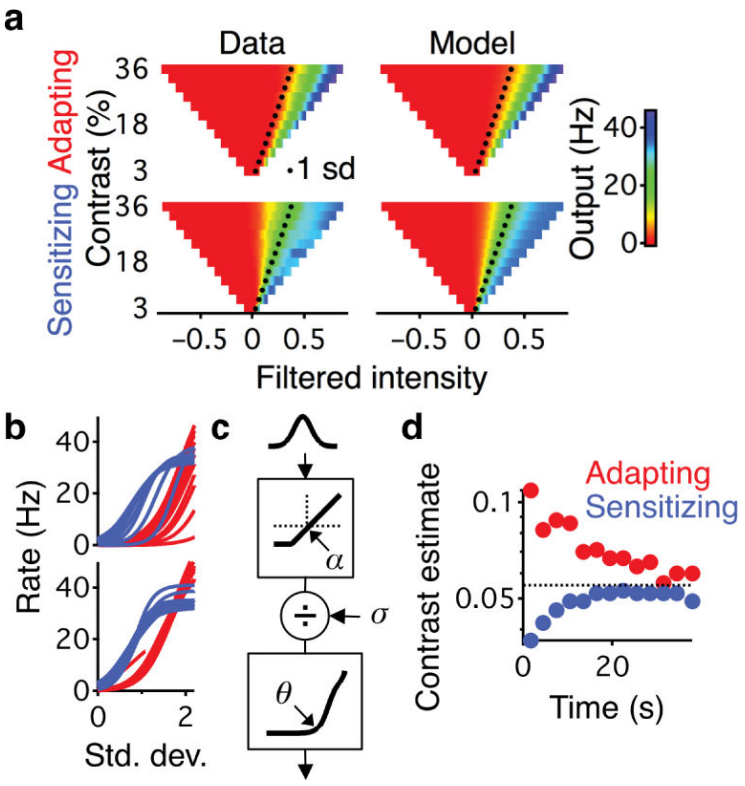

Figure 4.

Sensitizing cells specialize to encode weak signals; adapting cells encode strong signals. (**a**) Twelve different contrast levels (3 – 36 %) were randomly interleaved for at least 110 s and three repeats, and the first 10 s of data in each contrast was discarded. Nonlinearities are shown for an adapting (top) and sensitizing (bottom) cell for the different contrasts. Each row is a different nonlinearity, displayed in a color scale. Black dots indicate one standard deviation above the mean for each contrast level. Nonlinearities calculated from the data (left), and as predicted using a model described in panel (**c**) (right). (**b**) Normalized nonlinearities from cells in panel (**a**). For each contrast, the nonlinearity was scaled along the abscissa by the input standard deviation (top) or shifted by a common factor (α) and then scaled along the abscissa by the contrast (bottom). (**c**) Model M_α. Input values were passed through a threshold function, which shifted the mean value by a factor, α, then were rescaled by the contrast (σ), and then passed through a secondary nonlinearity with threshold θ to recreate the range of nonlinearities shown in (**a**). The secondary nonlinearity is the average nonlinearity for a cell after shifting by α and rescaling. (**d**) Nonlinearities N_i (g) were computed for each 3 s bin. For each bin, an estimate of the contrast was determined as the contrast σ for which the steady-state nonlinearity of the model M_α (σ) had the smallest mean-squared difference to N_i (g). Low contrast (5 %) followed 40 s of high contrast (35 %).

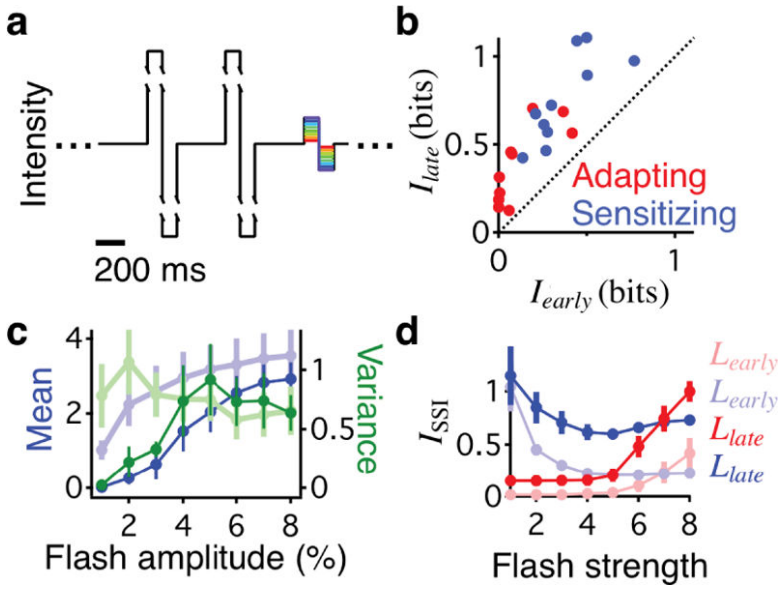

Figure 5.

Sensitizing and adapting cells increase information transmission using opposing changes in firing rate. (**a**) Stimulus used in the calculation of mutual information and the stimulus specific information (SSI) for low contrast. 20 s of identical high contrast pulses were followed by L_{early}, which was 2 s of 8 randomly presented low contrast pulses. For L_{late}, every 180 s, 44s seconds of continuous, randomly organized, low contrast pulses was presented. (**b**) Mutual information during L_{late} versus L_{early}. L_{late} occurred from 22 – 44 s after high contrast, and L_{early} occurred from 0.5 – 2 s after high contrast. All sensitizing cells had a higher firing rate during L_{early} than L_{late} (Supplementary Fig. 9a). A bin size of 150 ms was used, but the increase of information during low contrast is independent of bin size (Supplementary Fig. 9b). (**c**) Average mean and variance during L_{early} (lighter colors, thicker lines) and L_{late} (darker colors, thinner lines) for the sensitizing cells in (**b**), shown as a function of the stimulus pulse amplitude. **d**) Stimulus specific information I_{SSI} for each of the 8 different low contrast stimuli. In (**c**) and (**d**), flash amplitude is the Michelson contrast, $(I_{max} - I_{min})/(I_{max} + I_{min})$, of the 8 brief flashes in the low contrast stimulus.

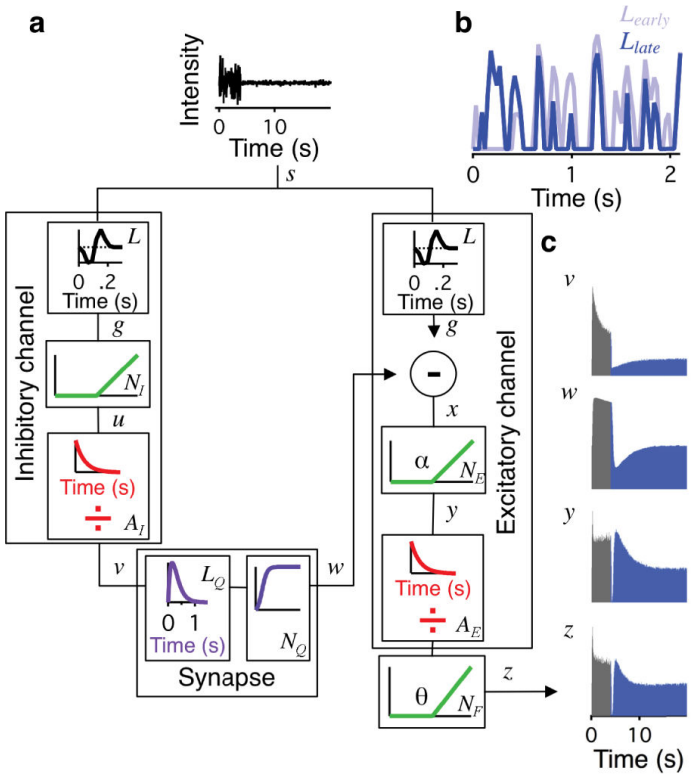

Figure 6.

Model of sensitization. (**a**) Sensitization results from the difference between two adapting pathways, one excitatory and one inhibitory. In each pathway, the stimulus is passed through a linear filter, *L*, a threshold, *N*, and then an adapting block, *A*. The adapting block is a feedforward module. In the inhibitory pathway, the input $u(t)$ is convolved with an exponential filter, F_A yielding $F_A * u$ (see methods). The input $u(t)$ is then divided by the filtered input $F_A * u$, such that the output of the adapting block $v(t)$ has a smaller amplitude than the input $u(t)$. A temporal filter, L_Q, and saturating function, N_Q, is applied to the inhibitory pathway before the two pathways are combined. (**b**) Response of the model to an input that repeated, and was identical during *Learly* and L_{late}. (**c**) Average responses over many white noise sequences, shown at different stages in the model. (*v*) In the inhibitory pathway, the response decreases during high contrast, and recovers during low contrast. (*w*) The synaptic functions decrease the response modulation during high contrast. (*y*) The decrease in inhibition at the transition to low contrast elevates activity in the excitatory pathway. (*z*) The final adapting block, A_E, in the excitatory pathway yields adaptation during high contrast, and preserves sensitization during low contrast.